Thermal Expansion Coefficient of Monolayer Molybdenum Disulfide Using Micro-Raman Spectroscopy

As Published: 10.1021/ACS.NANOLETT.9B01829

Publisher: American Chemical Society (ACS)

Persistent URL: https://hdl.handle.net/1721.1/134770

Version: Author's final manuscript: final author's manuscript post peer review, without publisher's formatting or copy editing

Thermal Expansion Coefficient of Monolayer Molybdenum Disulfide Using Micro-Raman Spectroscopy

Lenan Zhang, Zhengmao Lu, Youngsup Song, Lin Zhao, Bikram Bhatia, Kevin R. Bagnall, Evelyn N. Wang*

Department of Mechanical Engineering, Massachusetts Institute of Technology, Cambridge, MA 02139, USA

* Corresponding author: enwang@mit.edu

ABSTRACT

Atomically thin two-dimensional (2D) materials have shown great potential for applications in nanoscale electronic and optical devices. A fundamental property of these 2D flakes that needs to be well characterized is the thermal expansion coefficient (TEC), which is instrumental to the dry transfer process and thermal management of 2D material-based devices. Yet, most of current studies of 2D materials' TEC extensively rely on simulations due to the difficulty of performing experimental measurements on an atomically thin, micron-sized, and optically transparent 2D flake. In this work, we present a three-substrate approach to characterize the TEC of monolayer molybdenum disulfide (MoS_2) using micro-Raman spectroscopy. The temperature dependence of the Raman peak shift was characterized with three different substrate conditions, from which the in-plane TEC of monolayer MoS_2 was extracted based on lattice symmetries. Independently from two different phonon modes of MoS_2, we measured the in-plane TECs as $(7.6\pm0.9)\times10^{-6}$ 1/K and $(7.4\pm0.5)\times10^{-6}$ 1/K, respectively, which are in good agreement with previously reported values based on first principle calculations. Our work is not only useful for thermal mismatch reduction during material transfer or device operation, but provides a general experimental method that does not rely on simulations to study key properties of 2D materials.

KEYWORDS: 2D materials, MoS_2 monolayer, thermal expansion coefficient, micro-Raman spectroscopy, three-substrate approach, phonon deformation potential

Recent advances in atomically thin two-dimensional (2D) materials, such as graphene and transition-metal dichalcogenide (TMD) have attracted particular interest due to their exceptional properties[1–5] and promising applications in nanoscale devices.[6–11] It is of both fundamental and practical significance to understand the thermal expansion coefficient (TEC) of such materials. On one hand, TEC provides access to general anharmonic vibrational behavior of low-dimensional systems.[12,13] On the other hand, it is instrumental to reducing thermal mismatch, optimizing the dry transfer process, and avoiding device failure during operation.[14] However, direct measurements of the TEC of 2D materials remain limited to date for various reasons. (1) These atomically thin 2D materials are, more often than not, attached to thick substrates which unfortunately dominate the thermal expansion behavior. Even though it is possible to suspend the sample on microfabricated holes or slots (~10 μm^2 in area), the corresponding free expansion can hardly be observed. (2) Most 2D materials are optically transparent, which makes it difficult to measure the TEC using conventional optical approaches.[15] Accordingly, current understanding of the TEC for 2D materials relies on either pure theoretical calculations[16,17] or more recently, combining experimental characterization (such as electron energy-loss (EEL) spectroscopy[18]) with first-principle modeling which still depends on the choice of *ab initio* simulation methods.[12,16–18] In addition, Bao *et al.* characterized the TEC of a graphene membrane using scanning electron microscope, which utilized graphene's negative TEC to create a sagging membrane on a trench and finite element simulation to estimate the TEC of the trench.[19]

In this work, we propose a method that experimentally determines the TEC for 2D materials in which the only necessary input is the lattice symmetry group. Specifically, we use micro-Raman spectroscopy, which is capable of probing optical phonons at the microscale and is widely applied

to materials characterization and thermometry.[2,20–28] Raman spectroscopy has advantages to study the TEC of 2D materials as it can directly measure the phonon frequency shift due to the perturbation of the strain field induced by thermal expansion.[29] In particular, Yoon *et al.* reported the substrate effect on the phonon frequency shift of graphene and showed the coupling between the thermal stress and thermal expansion.[30] The negative TEC of graphene was measured which agrees well with Bao *et al.*'s measurement at room temperature.[30] However, Yoon *et al.*'s approach requires biaxial strain coefficient and intrinsic temperature coefficient as inputs, which necessitates additional experimental and theoretical efforts.[30] In this work, we propose a pure experimental approach to measure TEC that can decouple the effect of thermal stress, in-plane thermal expansion and out-of-plane thermal expansion effect on the Raman peak position and does not require theoretically computed parameters as inputs. As an example, we demonstrated the capability of our method by measuring the TEC of monolayer molybdenum disulfide (MoS_2). We chose MoS_2 monolayer since it is one of the most representative TMDs[3,4] which is widely used in nanoscale devices.[6–8] Many theoretical results of MoS_2 are also available to validate our approach.[16,17] We theoretically analyzed a temperature and stress dependent Raman spectrum of monolayer MoS_2 through the phonon deformation potential and group theory, which describes the effect of substrates on the supported 2D flakes. This unified theoretical framework was then used to decouple the thermal stress, in-plane and out-of-plane thermal expansion effect and guide the TEC measurement. Next, we extracted the TEC by characterizing the temperature-dependent Raman spectra of monolayer MoS_2 flakes which were transferred onto three different substrates: one suspended (or supported on an "air substrate"), one on fused silica, and another on copper. The measured TEC using this three-substrate method shows good agreement with previous theoretical calculations. This work presents a simple yet purely experimental method to measure

the TEC of monolayer MoS_2, which can also be widely applied to study the thermophysical properties of many other 2D materials and thin films.

We performed our measurements on single crystalline monolayer MoS_2 which was grown using chemical vapor deposition (CVD). The MoS_2 monolayer was characterized using optical and spectroscopic approaches (Section I of the Supporting Information for more details). Figure 1(a) shows an optical image of the MoS_2 flake over the 300 nm thick thermal oxide layer. The monolayer nature of this flake was confirmed by atomic force microscopy (AFM) characterization, where the thickness was determined to be about t = 1 nm (Figure 1(b)). As shown in Figure 1(c), monolayer MoS_2 has a hexagonal lattice structure which belongs to the D_{3h} point group.[25,31] Each unit cell consists of one molybdenum atom and two sulfur atoms. Consequently, monolayer MoS_2 has three Raman active optical phonon modes, *i.e.*, A_1', E' and E'' where the E'' mode is forbidden in the back-scattering configuration.[32] The A_1' mode represents the out-of-plane vibration of atoms whereas both E' and E'' modes represent the in-plane vibrations which have two-fold degeneracies (Figure 1(c)). Figure 1(d) shows a typical Raman spectrum of monolayer MoS_2 at room temperature where the characteristic peak positions of A_1' and E' modes are at about 405 cm^{-1} and 385 cm^{-1} respectively. According to the symmetry group of the lattice structure, the irreducible representation of the Raman active optical phonon modes Γ_{ph} at the Γ point can be decomposed as,[31]

$$\Gamma_{ph} = A_1' + E'. \quad (1)$$

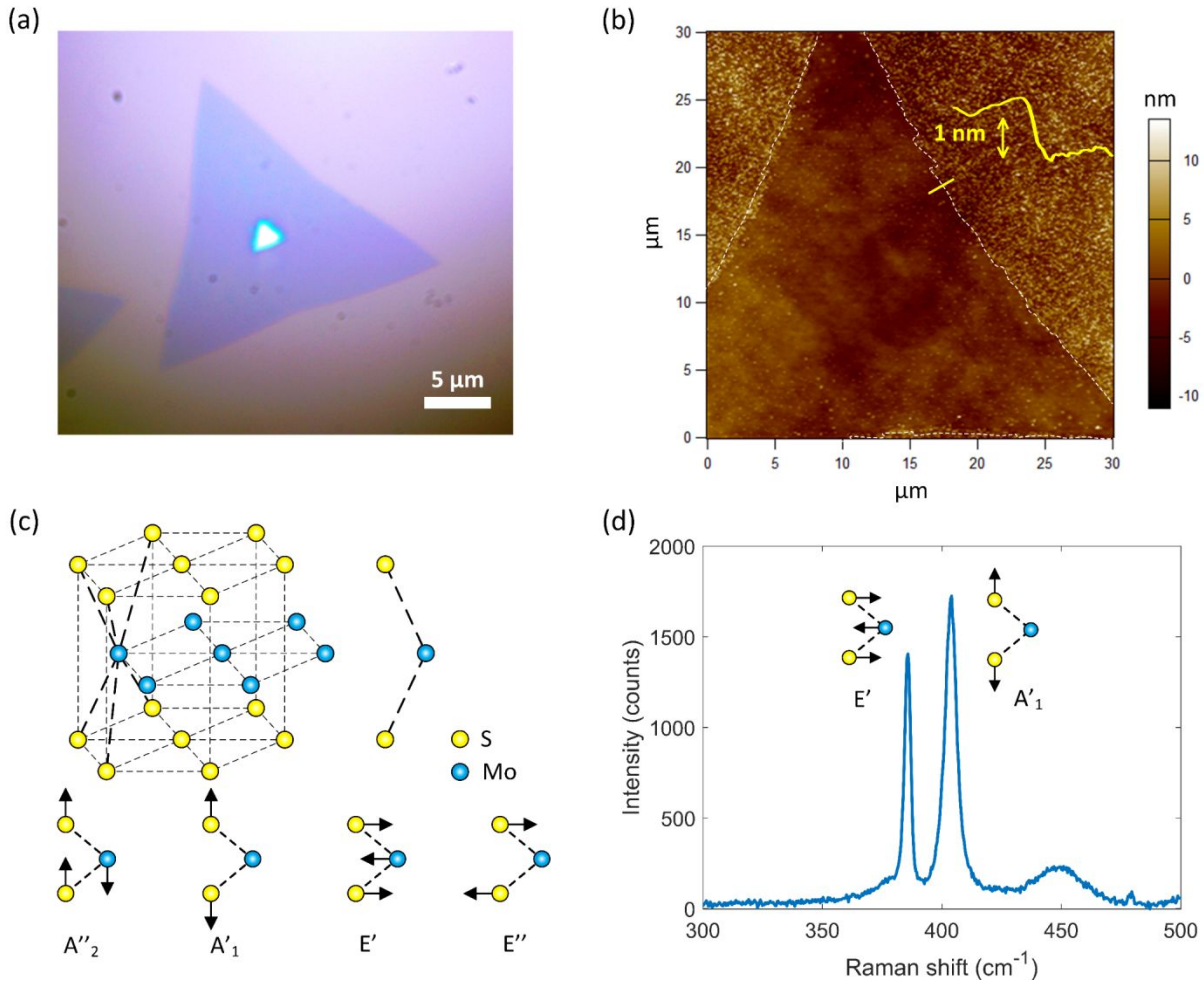

Figure 1 (a) Optical image of a CVD grown single crystalline monolayer MoS_2 flake on a 300 nm thick oxide layer from thermal oxidation of heavily doped silicon. The silicon substrate underneath is 1 mm thick. The bright small triangle at the center of the flake indicates the multilayer region which is more reflective than the monolayer region. (b) AFM image of a representative monolayer MoS_2 flake. Inset: The step height measurement from the monolayer to the substrate along the yellow line. The measurement results ($t \approx 1$ nm thickness) confirmed that the MoS_2 flake studied in this work is a single layer. (c) Lattice structure, unit cell, and Γ point phonon modes of the monolayer MoS_2. The monolayer MoS_2 belongs to the D_{3h} group. The A_1' (~405 cm^{-1}) and E' (~385 cm^{-1}) modes were detected in the backscattering configuration. (d)

Typical Raman spectrum of the monolayer MoS_2 flake on the thermal oxide substrate. Schematic shows the corresponding vibrational modes of A_1' and E' peaks.

To understand the role of TEC in the phonon frequency shift, we performed symmetry and perturbation analysis on the monolayer MoS_2. According to the basis functions of the D_{3h} group (see character table of D_{3h} group in Supporting Information Section II), the perturbation potential V under an arbitrary strain field $\{\varepsilon_{ij}\}$ can be explicitly expressed as,

$$V = \sum V_{ij}\,\varepsilon_{ij} = \frac{1}{2}\left(V_{xx} + V_{yy}\right)\left(\varepsilon_{xx} + \varepsilon_{yy}\right) + \frac{1}{2}\left(V_{xx} - V_{yy}\right)\left(\varepsilon_{xx} - \varepsilon_{yy}\right) + V_{zz}\,\varepsilon_{zz} + 2\left(V_{xy}\,\varepsilon_{xy} + V_{yz}\,\varepsilon_{yz} + V_{zx}\,\varepsilon_{zx}\right), \quad i,j = x,y\ or\ z, \tag{2}$$

where $\{\varepsilon_{ij}\}$ and $\{V_{ij}\}$ are the symmetric second rank tensors representing the strain perturbation and the corresponding deformation potentials, respectively. More specifically, the $V_{xx} + V_{yy}$ and V_{zz} terms belong to A_1', $V_{xx} - V_{yy}$ and V_{xy} belong to E', and V_{yz} and V_{zx} belong to E'', and therefore the perturbation potential V can be represented by $\Gamma_V = A_1' + E' + E''$. The shift of phonon frequency due to the perturbation potential V is given by the matrix element,[33]

$$\Delta\omega^{(n)} = \frac{1}{\hbar}\langle\Gamma^{(n)}|V|\Gamma^{(n)}\rangle, \quad n = A_1'\ or\ E' \tag{3}$$

where $\Delta\omega^{(n)}$ is the change of phonon frequency of A_1' or E' mode, $\Gamma^{(n)}$ is the corresponding wavefunction, and $\hbar$ is the reduced Planck's constant. Plugging Eq. (2) into Eq. (3) and applying

orthogonality relationships (*i.e.*, calculating the direct product $\Gamma_{ph}\otimes\Gamma_V$),[33] Eq. (3) can be further simplified as (see Supporting Information Section II for detailed derivations),

$$\Delta\omega^{A_1'} = a^{A_1'}(\varepsilon_{xx} + \varepsilon_{yy}) + b^{A_1'}\varepsilon_{zz} \tag{4}$$

$$\Delta\omega^{E'} = a^{E'}(\varepsilon_{xx} + \varepsilon_{yy}) + b^{E'}\varepsilon_{zz} \pm c^{E'}\left[(\varepsilon_{xx} - \varepsilon_{yy})^2 + 4\varepsilon_{xy}^2\right]^{\frac{1}{2}} \tag{5}$$

where $a^{A_1'}$ and $b^{A_1'}$ are the phonon deformation potential constants (PDP) of the A_1' mode, and $a^{E'}$, $b^{E'}$ and $c^{E'}$ are the PDP of the E' mode. The $\pm$ shown in Eq. (5) arises from the two-fold degeneracy of the E' mode. As $\{\varepsilon_{ij}\}$ is related to the thermal expansion and mechanical stress through the constitutive relation, we can obtain the general expressions describing the temperature and stress dependent phonon frequency (see Eqs. S(6) and S(8) in the Supporting Information). Note that the above analysis is valid for most of the TMD monolayers that belong to the D_{3h} point group (such as $MoSe_2$, $MoTe_2$, WS_2 and WSe_2). Additionally, for other symmetry point groups, this general theoretical framework still applies as we change the phonon modes and perturbation potential accordingly. In the thermal measurement, all of the stresses arose from thermal mismatch as no external mechanical forces were applied.[34] Accordingly, the MoS_2 flake was in a biaxial stress state with equal in-plane normal stress components ($\sigma_{xx} = \sigma_{yy} = \sigma$) and negligible shear stress ($\sigma_{xy} \approx 0$). In addition, the normal stress component σ_{zz} was negligible because the top of the flake was free to expand along c-axis. Consequently, we obtained the phonon frequency shift as a function of the in-plane thermal stress σ and temperature rise ΔT:

$$\Delta\omega^{(n)} = K^{(n)}\sigma + A^{(n)}\Delta T, \quad n = A_1' \text{ or } E' \tag{6}$$

where $K^{(n)}$ is known as the biaxial stress coefficient of A_1' or E' mode, and $A^{(n)}$ represents the temperature coefficients of the corresponding modes. It can be clearly seen from Eq. (6) that the thermal expansion can affect the phonon frequency through both the in-plane thermal stress σ and the temperature coefficient $A^{(n)}$. In this work, we eliminated the need to know the thermal stress σ or the biaxial stress coefficient $K^{(n)}$ from Eq. (6) using a three-substrate method.

Figure 2 shows the concept of the three-substrate method. The single crystalline monolayer MoS_2 flake was firstly transferred to a substrate consisting of 300 nm thick thermal oxide and 1 mm thick silicon with holes patterned in it (see Figure 2(a)). The diameter of the hole is D = 5 μm. As the suspended MoS_2 monolayer has a very large aspect ratio ($D/t \approx 5000$), the possible compressive stress can be relaxed through buckling. Thus, the suspended area should be nearly free-of-stress (see Supporting Information Section III for detailed assessment of the stress-free condition).[2,20–22] Since this region (on the 5 μm diameter hole) is larger than the laser spot size (≈1 μm), we can perform the temperature-dependent Raman measurements and obtain the temperature coefficient $A^{(n)}$. Next, monolayer MoS_2 flakes were transferred onto 1 mm thick fused silica substrate (MolTech GmbH Molecular Technology) and 1 mm thick pure copper (99.999% purity, CU-M-05-WF American Elements) wafers, respectively (Figures 2(b) and (c)). As the fused silica has very low TEC ($\alpha_{SiO_2} = 0.55 \times 10^{-6}\ 1/K$), compressive thermal stress $\sigma_{SiO_2} < 0$ was induced within the MoS_2 flakes when temperature rose. On the other hand, the thermal mismatch due to the very high TEC of pure copper ($\alpha_{Cu} = 16.5 \times 10^{-6}\ 1/K$) led to tensile stress $\sigma_{cu} > 0$ acting on the MoS_2 flakes. Since the supporting substrates were much thicker than the MoS_2 flakes, *i.e.*, 1 mm $\gg$ 1 nm, the substrates experienced free expansion with temperature rise. Note that no slip

between the MoS_2 flakes and the substrates is expected when the strain rate was relatively low due to the strong van der Waals (vdW) interaction (see Supporting Information Section III for detailed assessment of the no-slip condition).[22,35,36] The strain-stress relations of the flakes supported on different substrates can be expressed as

$$\varepsilon_{SiO2} = \alpha\Delta T + \frac{1-\nu}{E}\sigma_{SiO_2} = \alpha_{SiO_2}\Delta T \tag{7}$$

$$\varepsilon_{Cu} = \alpha\Delta T + \frac{1-\nu}{E}\sigma_{Cu} = \alpha_{Cu}\Delta T \tag{8}$$

where ε_{SiO2} and ε_{Cu} are the in-plane thermal strain within the MoS_2 flake when they were supported by fused silica and pure copper substrates respectively. σ_{SiO_2} and σ_{Cu} are the corresponding in-plane thermal stress within the flake on the fused silica and pure copper substrates, which were induced by the thermal mismatches. α, E, and ν represent the in-plane TEC, Young's modulus, and Poisson ratio of the monolayer MoS_2 flake, respectively. Inserting Eqs. (7) and (8) into Eq. (6), the effect of TEC on phonon frequency shift through thermal stresses σ_{SiO_2} and σ_{Cu} can be explicitly shown as,

$$\Delta\omega_{SiO_2}^{(n)} = \left(\frac{K^{(n)}(\alpha_{SiO_2}-\alpha)E}{1-\nu} + A^{(n)}\right)\Delta T = A_{SiO_2}^{(n)}\Delta T, \quad n = A_1' \; or \; E' \tag{9}$$

$$\Delta\omega_{Cu}^{(n)} = \left(\frac{K^{(n)}(\alpha_{Cu}-\alpha)E}{1-\nu} + A^{(n)}\right)\Delta T = A_{Cu}^{(n)}\Delta T, \quad n = A_1' \; or \; E'. \tag{10}$$

Eqs. (9) and (10) suggest that we can relate the TEC to temperature coefficients of Raman measurements ($A_{SiO_2}^{(n)}$and $A_{Cu}^{(n)}$) and eliminate the biaxial stress coefficient $K^{(n)}$. Further, for each symmetry class, we can explicitly express α as a function of $A_{SiO_2}^{(n)}$, $A_{Cu}^{(n)}$ and $A^{(n)}$ (Supporting Information II for detailed derivations):

$$\alpha = \frac{\left(A_{cu}^{(n)} - A^{(n)}\right)\alpha_{SiO_2} - \left(A_{SiO_2}^{(n)} - A^{(n)}\right)\alpha_{Cu}}{A_{cu}^{(n)} - A_{SiO_2}^{(n)}}, \quad n = A_1' \text{ or } E'. \tag{11}$$

where $A^{(n)}$, $A_{SiO_2}^{(n)}$, and $A_{cu}^{(n)}$ can all be determined experimentally and α_{SiO_2} and α_{Cu} are the bulk properties (characterized by the substrate suppliers in this work). Eq. (11) also suggests that we can obtain the in-plane TEC from either the A_1' or E' mode independently. Since α determined from different modes should ideally be the same, this was used as a criterion to assess the consistency of our method.

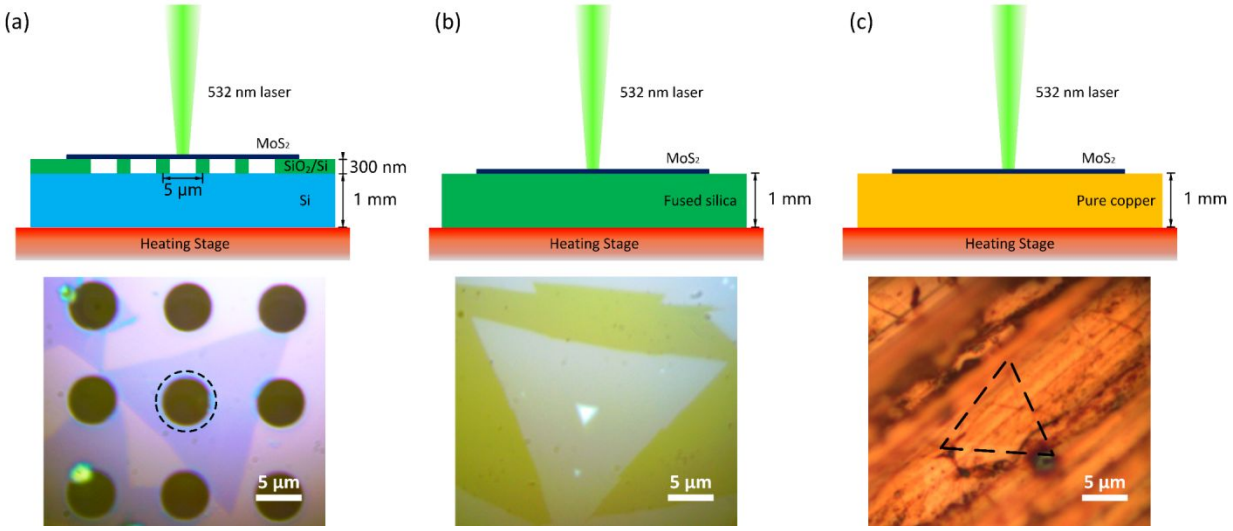

Figure 2 Schematics of the concept of three-substrate method for TEC characterization. (a) Temperature-dependent Raman measurement on monolayer MoS_2 suspended over 5 μm diameter holes. Bottom: 100X magnification optical image of a monolayer MoS_2 flake transferred onto the holey substrate. The dashed-circle indicates the suspended free expansion area where the measurement was performed. (b) Temperature-dependent Raman measurement on monolayer MoS_2 supported by a 1 mm-thick fused silica substrate. Bottom: 100X magnification optical image of a monolayer MoS_2 flake transferred onto the fused silica substrate. (c) Temperature-dependent

Raman measurement on monolayer MoS_2 supported by a 1 mm-thick pure copper substrate. Bottom: 100X magnification optical image of a monolayer MoS_2 flake transferred onto pure copper substrate. The dashed-triangle indicates the position of the flake (see Figure S1 for details).

The temperature-dependent Raman measurements were performed to characterize the temperature coefficients for different substrates (Supporting Information Section IV for details about the micro-Raman system). The Raman scattering was excited by a 532 nm wavelength diode laser (05-01 series, Cobolt). The 100X, $NA = 0.8$ microscope objective (LMPlanFL N, Olympus) was used to focus the laser excitation and collect the Raman scattering. The corresponding laser spot size was ≈1 μm. The laser power was maintained at < 0.1 mW for the suspended flakes measurement and at < 1 mW for the supported flakes measurements to avoid excessive laser heating. The samples were heated by a temperature control stage with 0.01 ℃ stability (HCP621 V, Instec). Raman peak positions were measured with temperature increasing from 20 ℃ to 200 ℃ for both the suspended and fused silica supported sample. The pure copper supported flakes were heated up to 160 ℃ to avoid copper oxidation. Figure 3 shows that the Raman peak positions of A_1' and E' modes vary with the temperature rise on different substrates. Variations of the peak position at 20 ℃ can be seen on different substrates which is attributed to the residual stress during sample preparation. However, these variations only affect the bias of the temperature dependent phonon frequency curve and do not change the intrinsic and substrate dependent temperature coefficients (see Supporting Information V for detailed explanations). The corresponding temperature coefficients extracted using linear fitting are listed in Table 1. The effect of thermal stress on the phonon frequency shift was confirmed experimentally. The temperature coefficients of the suspended

MoS_2 flakes were $A^{A_1'} = -0.0148 \pm 0.0001\ cm^{-1}/K$ and $A^{E'} = -0.0145 \pm 0.0002\ cm^{-1}/K$, which agrees with previously reported values.[20,32,37] For the A_1' mode, the temperature coefficient changed to $-0.0125 \pm 0.0002\ cm^{-1}/K$ when the MoS_2 flakes were transferred to the fused silica substrate (see Figures 3(a) and (b)), indicating a compressive thermal stress acting on the flakes according to Eqs. (6) and (9). On the pure copper substrate, however, the temperature coefficient became $-0.0177 \pm 0.0005\ cm^{-1}/K$ due to the tensile thermal stress (see Eqs. (6) and (10)). Similar trends were found for the E' mode as well (Table 1). The no-slip condition mentioned above was also confirmed through the temperature-dependent Raman measurements, since the temperature coefficient highly depends on the TEC of the substrate and no kinks were observed in Figure 3 (see Supporting Information Section III for detailed analysis). In addition, it is worth noting that the change of temperature coefficients due to the in-plane thermal stress for the E' mode was more significant than that for the A_1' mode because the in-plane vibrational mode E' was more sensitive to the in-plane perturbation than the out-of-plane vibrational mode A_1'. Using Eq. (11), the in-plane TEC of monolayer MoS_2 was $(7.6 \pm 0.9) \times 10^{-6}\ 1/K$ determined from the A_1' mode, while using E' mode resulted in $(7.4 \pm 0.5) \times 10^{-6}\ 1/K$. The agreement between these two independent calculations demonstrates the consistency of the proposed method. Note that measurements from the E' mode had smaller uncertainty because the change of temperature coefficients of E' mode is larger than that of A_1' mode (Supporting Information Section VI for uncertainty analysis).

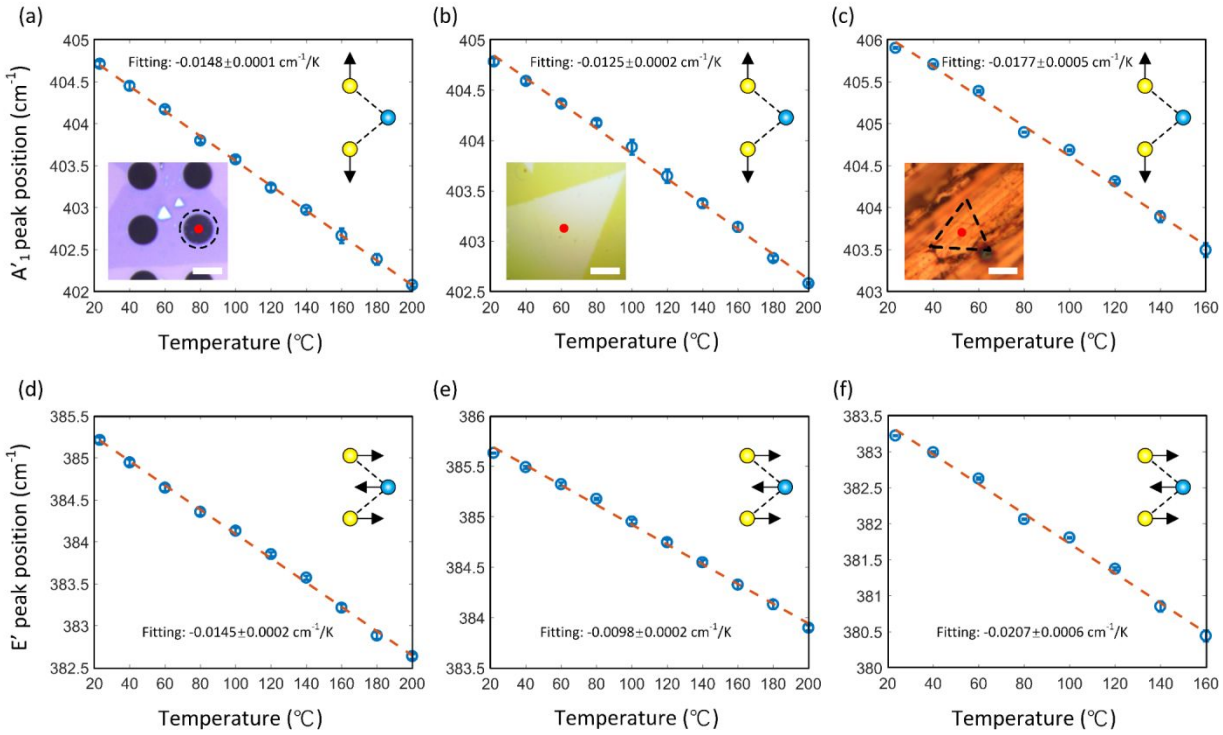

Figure 3 Temperature-dependent Raman measurements for A_1' and E' modes on different substrates. (a)-(c) Raman peak position of A_1' mode as a function of temperature on (a) suspended, (b) fused silica supported and (c) pure copper supported monolayer MoS_2 flakes. Inset: schematic of the out-of-plane A_1' vibrational mode. Inset: 100X magnification optical images the monolayer MoS_2 flakes on three corresponding substrates. Scale bars represent 5 μm. The red dots indicate where the laser excitation was focused. (d)-(e) Raman peak position of E' mode as a function of temperature on (d) suspended, (e) fused silica supported and (f) pure copper supported monolayer MoS_2 flakes. Inset: schematic of the in-plane E' vibrational mode. The y-axis error bars represent random errors from multiple measurements.

Table 1. Temperature coefficients for A_1' and E' optical phonon modes of single crystalline monolayer MoS_2 flakes on different substrates.

MoS_2 samples	$A^{A_1'}$ (cm^{-1}/K)	$A^{E'}$ (cm^{-1}/K)
suspended	-0.0148±0.0001	-0.0145±0.0002
fused silica supported	-0.0125±0.0002	-0.0098±0.0002
pure copper supported	-0.0177±0.0005	-0.0207±0.0006
glass supported	-0.0152±0.0004	-0.0151±0.0003

Moreover, we transferred the MoS_2 flakes on a glass substrate which has the TEC ranging from $7.5 \times 10^{-6}\ 1/K$ to $8.5 \times 10^{-6}\ 1/K$,[38] very close to the TEC of monolayer MoS_2 measured in this work. Based on the TEC of monolayer MoS_2 reported with our method, the thermal mismatch is minimal in this case. Therefore, we expect the temperature coefficients to be very similar to the one measured on the suspended flakes, which we confirmed with experimental data (row 5 of Table 1). This result further validates our three-substrate method (see Supporting Information Section VII for details of the measurement result and full analysis). We compared our measurement results with literature values listed in Table 2. Previous theoretical calculations used different density functional theory (DFT) methods such as the quasi-harmonic approximation (QHA) method[12,16,18,39,40] and the symmetry-preserving deformations (SPD) method.[17] As shown in Table 2, the calculated TEC varied from $6.7 \times 10^{-6}\ 1/K$ to $7.3 \times 10^{-6}\ 1/K$ depending on the choice of computation method, which shows excellent agreement with our measurement. The measured TEC of MoS_2 monolayer is larger than the bulk value ($4.9 \times 10^{-6}\ 1/K$) characterized by Murray and Evans[41] due to the absence of the interlayer vdW interaction, which is an agreement with the theoretical prediction by Gan *et al*.[17] However, the unusually high TEC of the MoS_2 monolayer ($64.9 \times 10^{-6}\ 1/K$) reported in Hu *et al*'s work[18] was not observed in our measurement. Since our approach might be further extended to study the TEC of other thin films or 2D materials

including those belonging to D_{3h} point group and other symmetry groups, we list experimentally measured temperature coefficients by other works for reference (Supporting Information Section VIII).

Table 2. Comparison of the in-plane TEC of monolayer MoS_2 obtained from this work and previous literature presented data.

References	Methods	TECs (10^{-6} 1/K)
Sevik (2014)[16]	DFT-QHA (theoretical)	7.2
Huang *et al.* (2014)[39]	DFT-QHA (theoretical)	7.2
Gan *et al.* (2016)[17]	DFT-SPD (theoretical)	6.7
Wang *et al.* (2015)[40]	DFT-QHA (theoretical)	7.3
This work	Micro-Raman (experimental)	7.6±0.9 (A_1'), 7.4±0.5 (E')

In summary, we proposed an experimental approach to measure the in-plane TEC of 2D materials and demonstrated its application by measuring the monolayer MoS_2 flakes. Based on symmetry analysis, we showed that the TEC can affect the Γ point optical phonon frequency through both the in-plane thermal stress and temperature coefficients due to the contribution of thermal mismatch and free expansion, respectively. We decoupled these two effects using the three-substrate method, where the monolayer flakes were transferred on a holey substrate, fused silica substrate, and pure copper substrate. Temperature-dependent Raman measurements were carried out on all three substrates, and the corresponding temperature coefficients for each mode were characterized. We extracted the in-plane TEC from two different phonon modes, *i.e.*, A_1' and E', independently and showed consistent results. The TEC that we measured in this work agrees well

with previously reported values obtained from theoretical or semi-experimental approaches. We demonstrated a useful method for thermal mismatch analysis of MoS_2 based devices. More specifically, our procedure involves: (1) deriving the temperature and stress dependent phonon frequency based on crystal symmetry; (2) obtaining the expression for the TEC of 2D flakes with three carefully chosen substrates; (3) performing temperature-dependent Raman measurement on the three substrates to solve for the coefficients. This is a general framework for TEC measurement that can be applied to many other 2D materials or thin films.

ASSOCIATED CONTENT

Supporting Information

The Supporting Information is available free of charge on the ACS Publications website at DOI:

Single crystalline monolayer MoS_2 preparation and characterization, temperature and stress dependent phonon frequency analysis of monolayer MoS_2, micro-Raman spectroscopy experimental setup, uncertainty analysis of experimental results, and temperature-dependent micro-Raman study on the glass substrate

AUTHOR INFORMATION

Corresponding Author

*E-mail: enwang@mit.edu

ACKNOWLEDGEMENT

L. Zhang gratefully acknowledges funding support from the MIT/MTL GaN Energy Initiative and the Singapore-MIT Alliance for Research and Technology (SMART) LEES Program. Z. Lu acknowledges funding support from the Air Force Office of Scientific Research with Dr. Ali Sayir as the program manager under Award No. FA9550-15-1-0310.

REFERENCES

1. Geim, A. K.; Novoselov, K. S. The Rise of Graphene. *Nat. Mater.* **2007**, *6*, 183
2. Balandin, A. A.; Ghosh, S.; Bao, W.; Calizo, I.; Teweldebrhan, D.; Miao, F.; Lau, C. N. Superior Thermal Conductivity of Single-Layer Graphene. *Nano Lett.* **2008,** 8, 902-907.
3. Manzeli, S.; Ovchinnikov, D.; Pasquier, D.; Yazyev, O. V.; Kis, A. 2D Transition Metal Dichalcogenides. *Nature Reviews Materials* **2017,** 2, 17033.
4. Butler, S. Z.; Hollen, S. M.; Cao, L.; Cui, Y.; Gupta, J. A.; Gutiérrez, H. R.; Heinz, T. F.; Hong, S. S.; Huang, J.; Ismach, A. F.; Johnston-Halperin, E.; Kuno, M.; Plashnitsa, V. V.; Robinson, R. D.; Ruoff, R. S.; Salahuddin, S.; Shan, J.; Shi, L.; Spencer, M. G.; Terrones, M.; Windl, W.; Goldberger, J. E. Progress, Challenges, and Opportunities in Two-Dimensional Materials Beyond Graphene. *ACS Nano* **2013,** 7, 2898-2926.
5. Guo, L.; Wu, M.; Cao, T.; Monahan, D. M.; Lee, Y.-H.; Louie, S. G.; Fleming, G. R. Exchange-Driven Intravalley Mixing of Excitons in Monolayer Transition Metal Dichalcogenides. *Nat. Phys.* **2019,** 15, 228.
6. Fiori, G.; Bonaccorso, F.; Iannaccone, G.; Palacios, T.; Neumaier, D.; Seabaugh, A.; Banerjee, S. K.; Colombo, L. Electronics Based on Two-Dimensional Materials. *Nat. Nanotechnol.* **2014,** 9, 768.
7. Wang, Q. H.; Kalantar-Zadeh, K.; Kis, A.; Coleman, J. N.; Strano, M. S. Electronics and Optoelectronics of Two-Dimensional Transition Metal Dichalcogenides. *Nat. Nanotechnol.* **2012,** 7, 699.
8. Radisavljevic, B.; Radenovic, A.; Brivio, J.; Giacometti, V.; Kis, A. Single-Layer MoS_2 Transistors. *Nat. Nanotechnol.* **2011,** 6, 147.
9. Han, W.; Kawakami, R. K.; Gmitra, M.; Fabian, J. Graphene Spintronics. *Nat. Nanotechnol.* **2014,** 9, 794.
10. Das, S.; Prakash, A.; Salazar, R.; Appenzeller, J. Toward Low-Power Electronics: Tunneling Phenomena in Transition Metal Dichalcogenides. *ACS Nano* **2014,** 8, 1681-1689.
11. Ling, X.; Lin, Y.; Ma, Q.; Wang, Z.; Song, Y.; Yu, L.; Huang, S.; Fang, W.; Zhang, X.; Hsu, A. L. Parallel Stitching of 2D Materials. *Adv. Mater.* **2016,** 28, 2322-2329.

12. Late, D. J.; Shirodkar, S. N.; Waghmare, U. V.; Dravid, V. P.; Rao, C. Thermal Expansion, Anharmonicity and Temperature-Dependent Raman Spectra of Single- and Few-Layer $MoSe_2$ and WSe_2. *ChemPhysChem* **2014,** 15, 1592-1598.
13. Su, L.; Zhang, Y.; Yu, Y.; Cao, L. Dependence of Coupling of Quasi 2-D MoS_2 with Substrates on Substrate Types, Probed by Temperature Dependent Raman Scattering. *Nanoscale* **2014,** 6, 4920-4927.
14. Yan, Z.; Liu, G.; Khan, J. M.; Balandin, A. A. Graphene Quilts for Thermal Management of High-Power GaN Transistors. *Nat. Commun.* **2012,** 3, 827.
15. James, J.; Spittle, J.; Brown, S.; Evans, R. A Review of Measurement Techniques for the Thermal Expansion Coefficient of Metals and Alloys at Elevated Temperatures. *Meas. Sci. Technol.* **2001,** 12, R1.
16. Sevik, C. Assessment on Lattice Thermal Properties of Two-Dimensional Honeycomb Structures: Graphene, h -BN, h -MoS_2, and h -$MoSe_2$. *Phys. Rev. B* **2014,** 89, 035422.
17. Gan, C. K.; Liu, Y. Y. F. Direct Calculation of the Linear Thermal Expansion Coefficients of MoS_2 *via* Symmetry-Preserving Deformations. *Phys. Rev. B* **2016,** 94, 134303.
18. Hu, X.; Yasaei, P.; Jokisaari, J.; Öğüt, S.; Salehi-Khojin, A.; Klie, R. F. Mapping Thermal Expansion Coefficients in Freestanding 2D Materials at the Nanometer Scale. *Phys. Rev. Lett.* **2018,** 120, 055902.
19. Bao, W.; Miao, F.; Chen, Z.; Zhang, H.; Jang, W.; Dames, C.; Lau, C. N. Controlled Ripple Texturing of Suspended Graphene and Ultrathin Graphite Membranes. *Nat. Nanotechnol.* **2009,** 4, 562.
20. Yan, R.; Simpson, J. R.; Bertolazzi, S.; Brivio, J.; Watson, M.; Wu, X.; Kis, A.; Luo, T.; Hight Walker, A. R.; Xing, H. G. Thermal Conductivity of Monolayer Molybdenum Disulfide Obtained from Temperature-Dependent Raman Spectroscopy. *ACS Nano* **2014,** 8, 986-993.
21. Luo, Z.; Maassen, J.; Deng, Y.; Du, Y.; Garrelts, R. P.; Lundstrom, M. S.; Peide, D. Y.; Xu, X. Anisotropic In-Plane Thermal Conductivity Observed in Few-Layer Black Phosphorus. *Nat. Commun.* **2015,** 6, 8572.
22. Luo, Z.; Tian, J.; Huang, S.; Srinivasan, M.; Maassen, J.; Chen, Y. P.; Xu, X. Large Enhancement of Thermal Conductivity and Lorenz Number in Topological Insulator Thin Films. *ACS Nano* **2018,** 12, 1120-1127.
23. Cai, W.; Moore, A. L.; Zhu, Y.; Li, X.; Chen, S.; Shi, L.; Ruoff, R. S. Thermal Transport in Suspended and Supported Monolayer Graphene Grown by Chemical Vapor Deposition. *Nano Lett.* **2010,** 10, 1645-1651.
24. Yalon, E.; Aslan, Ö. B.; Smithe, K. K. H.; McClellan, C. J.; Suryavanshi, S. V.; Xiong, F.; Sood, A.; Neumann, C. M.; Xu, X.; Goodson, K. E.; Heinz, T. F.; Pop, E. Temperature-Dependent Thermal Boundary Conductance of Monolayer MoS_2 by Raman Thermometry. *ACS Appl. Mater. Interfaces* **2017,** 9, 43013-43020.
25. Huang, S.; Liang, L.; Ling, X.; Puretzky, A. A.; Geohegan, D. B.; Sumpter, B. G.; Kong, J.; Meunier, V.; Dresselhaus, M. S. Low-Frequency Interlayer Raman Modes to Probe Interface of Twisted Bilayer MoS_2. *Nano Lett.* **2016,** 16, 1435-1444.
26. Late, D. J. Temperature Dependent Phonon Shifts in Few-Layer Black Phosphorus. *ACS Appl. Mater. Interfaces* **2015,** 7, 5857-5862.
27. Pawbake, A. S.; Island, J. O.; Flores, E.; Ares, J. R.; Sanchez, C.; Ferrer, I. J.; Jadkar, S. R.; van der Zant, H. S. J.; Castellanos-Gomez, A.; Late, D. J. Temperature-Dependent Raman Spectroscopy of Titanium Trisulfide (TiS_3) Nanoribbons and Nanosheets. *ACS Appl. Mater. Interfaces* **2015,** 7, 24185-24190.

28. M, T.; Late, D. J. Temperature Dependent Phonon Shifts in Single-Layer WS_2. *ACS Appl. Mater. Interfaces* **2014,** 6, 1158-1163.
29. Rice, C.; Young, R. J.; Zan, R.; Bangert, U.; Wolverson, D.; Georgiou, T.; Jalil, R.; Novoselov, K. S. Raman-Scattering Measurements and First-Principles Calculations of Strain-Induced Phonon Shifts in Monolayer MoS_2. *Phys. Rev. B* **2013,** 87, 081307.
30. Yoon, D.; Son, Y.-W.; Cheong, H. Negative Thermal Expansion Coefficient of Graphene Measured by Raman Spectroscopy. *Nano Lett.* **2011,** 11, 3227-3231.
31. Cai, Y.; Lan, J.; Zhang, G.; Zhang, Y.-W. Lattice Vibrational Modes and Phonon Thermal Conductivity of Monolayer MoS_2. *Phys. Rev. B* **2014,** 89, 035438.
32. Sahoo, S.; Gaur, A. P. S.; Ahmadi, M.; Guinel, M. J. F.; Katiyar, R. S. Temperature-Dependent Raman Studies and Thermal Conductivity of Few-Layer MoS_2. *J. Phys. Chem. C* **2013,** 117, 9042-9047.
33. Dresselhaus, M. S.; Dresselhaus, G.; Jorio, A., *Group theory: application to the physics of condensed matter*; Springer Science & Business Media: 2007.
34. Bagnall, K. R.; Moore, E. A.; Badescu, S. C.; Zhang, L.; Wang, E. N. Simultaneous Measurement of Temperature, Stress, and Electric Field in GaN HEMTs with Micro-Raman Spectroscopy. *Rev. Sci. Instrum.* **2017,** 88, 113111.
35. Bertolazzi, S.; Brivio, J.; Kis, A. Stretching and Breaking of Ultrathin MoS_2. *ACS Nano* **2011,** 5, 9703-9709.
36. Lee, C.; Wei, X.; Kysar, J. W.; Hone, J. Measurement of the Elastic Properties and Intrinsic Strength of Monolayer Graphene. *Science* **2008,** 321, 385-388.
37. Lanzillo, N. A.; Glen Birdwell, A.; Amani, M.; Crowne, F. J.; Shah, P. B.; Najmaei, S.; Liu, Z.; Ajayan, P. M.; Lou, J.; Dubey, M; Nayak, S. K.; O'Regan, T. P. Temperature-Dependent Phonon Shifts in Monolayer MoS_2. *Appl. Phys. Lett.* **2013,** 103, 093102.
38. Hidnert, P. Thermal Expansion of Five Selected Optical Glasses. *J. Res. Natl. Bur. Stand.* **1954,** 52, 311.
39. Huang, L. F.; Gong, P. L.; Zeng, Z. Correlation between Structure, Phonon Spectra, Thermal Expansion, and Thermomechanics of Single-Layer MoS_2. *Phys. Rev. B* **2014,** 90, 045409.
40. Wang, Z.-Y.; Zhou, Y.-L.; Wang, X.-Q.; Wang, F.; Sun, Q.; Guo, Z.-X.; Jia, Y. Effects of In-Plane Stiffness and Charge Transfer on Thermal Expansion of Monolayer Transition Metal Dichalcogenide. *Chin. Phys. B* **2015,** 24, 026510.
41. Murray, R.; Evans, B. The Thermal Expansion of 2H-MoS_2 and 2H-WSe_2 between 10 and 320 K. *J. Appl. Crystallogr.* **1979,** 12, 312-315.

TOC Graphic

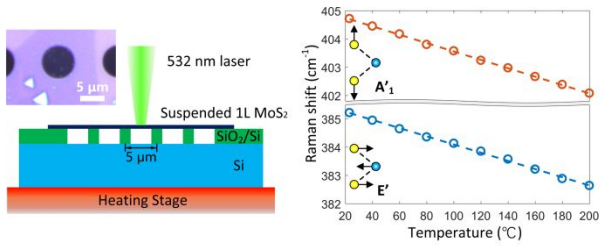
5 μm
532 nm laser
Suspended 1L MoS2
SiO2/Si
5 μm
Si
Heating Stage
Raman shift (cm-1)
A'1
E'
Temperature (℃)

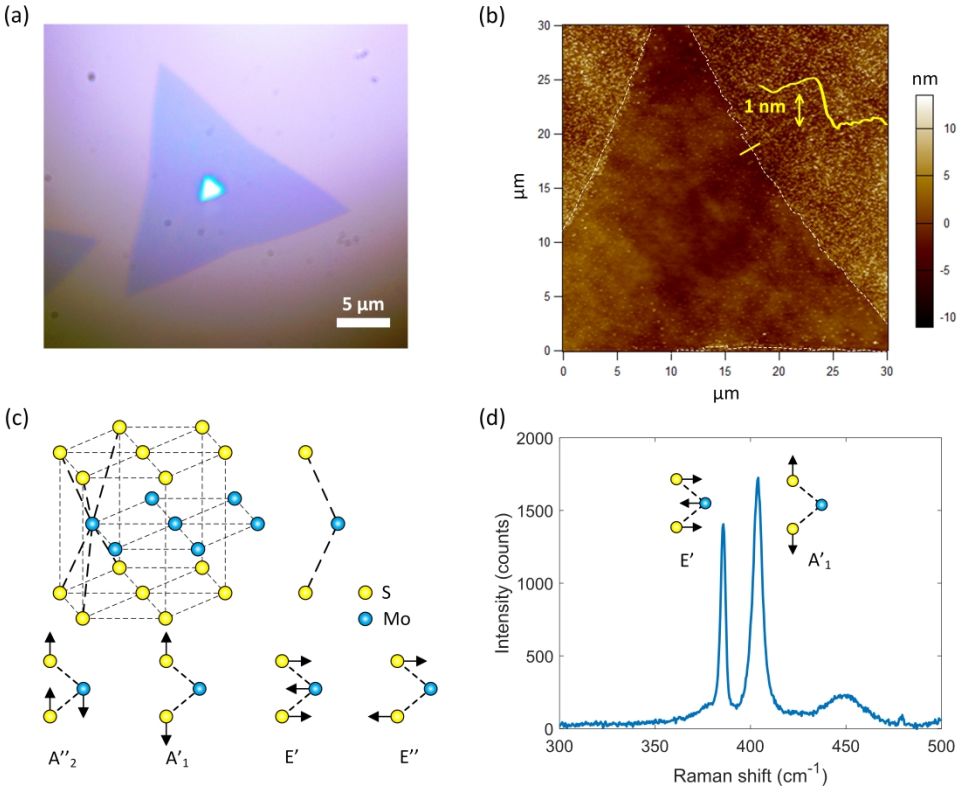

Figure 1

522x413mm (300 x 300 DPI)

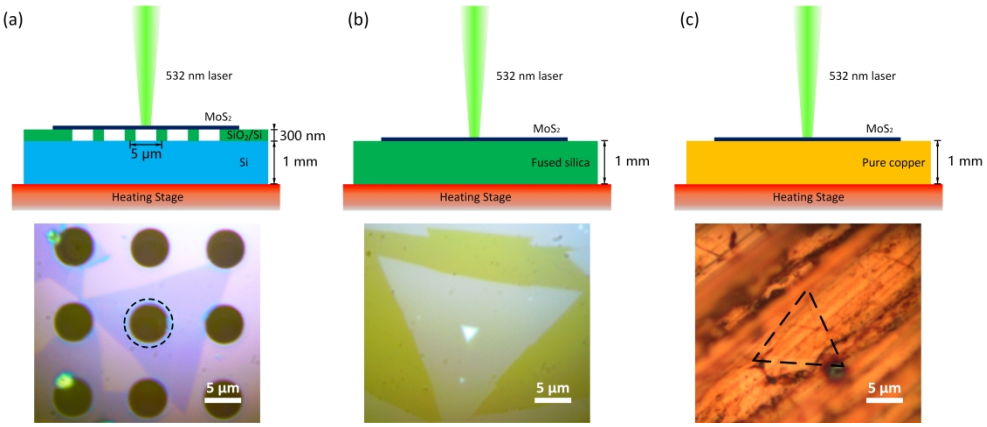

Figure 2

663x279mm (300 x 300 DPI)

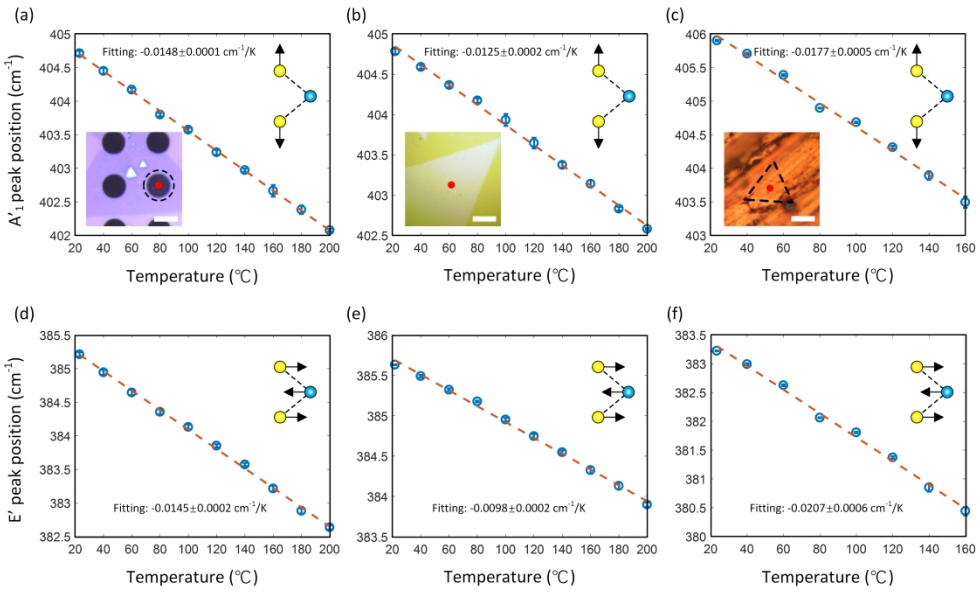

Figure 3

689x412mm (200 x 200 DPI)

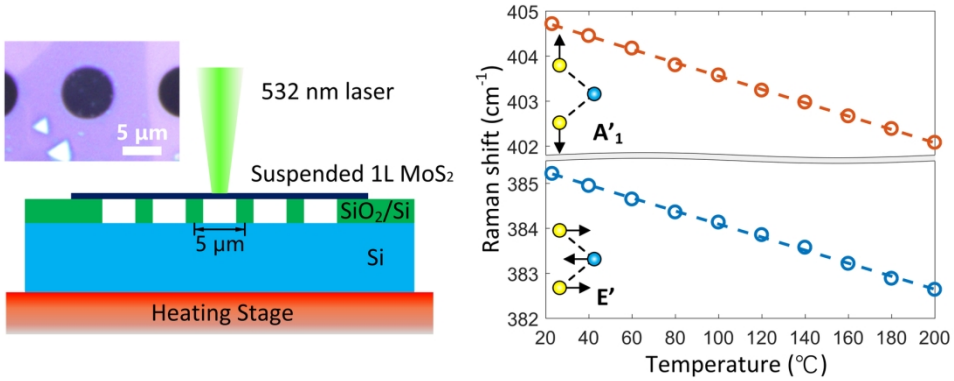

TOC graphic

82x33mm (600 x 600 DPI)